Applied Polymer SCIENCE

Nucleation Effect of Hydroxyl-Purified Multiwalled Carbon Nanotubes in Poly(*p*-phenylene sulfide) Composites

Jiang Sheng-Ling, Gu Xiao-Yu, Zhang Zhi-Yuan

Key Laboratory of Carbon Fiber and Functional Polymers Ministry of Education, P.O. Box 227, Beijing University of Chemical Technology, Beijing 100029, China

Correspondence to: G. Xiao-Yu (E-mail: guxy0818@163.com)

ABSTRACT: To investigate the nucleation effect of hydroxyl-purified multiwalled carbon nanotubes (MWNTs-OH) in poly(*p*-phenylenesulfide) (PPS), a series of composites were prepared by blending PPS with MWNTs-OH at 1, 2, and 3 wt %, respectively. Under SEM observation MWNTs-OH were found homogeneously dispersed in the PPS matrix. DSC thermograms revealed that the enthalpy (ΔH_c) of the composites increased with increasing MWNT-OH content, whereas the crystallization temperature (T_c) decreased progressively. The decrease in T_c was in accordance with the smaller crystallite size determined with WXRD characterization, and the increase in ΔH_c was evidenced by FTIR and XPS analyses. The higher ΔH_c shows that MWNTs-OH serves as a nucleating agent, providing sufficiently multiplied sites for crystal growth. The lowering of T_c was attributed not only to MWNTs-OH network hindrance to PPS chain fusing rearrangement, but also to a poorer affinity between MWNTs-OH and PPS; both effects coordinately govern T_c of PPS/MWNTs-OH composites. © 2012 Wiley Periodicals, Inc. J. Appl. Polym. Sci. 000: 000–000, 2012

KEYWORDS: poly(*p*-phenylene sulfide) (PPS); hydroxy purified multiwall carbon nanotubes; crystallization behavior

Received 12 July 2011; accepted 10 April 2012; published online
DOI: 10.1002/app.37870

INTRODUCTION

Poly(*p*-phenylene sulfide) (PPS) can be used as engineering plastics with excellent performances in heat stability, flame and chemical resistance, and size stability at high temperature,[1] but it bears the disadvantage of relatively low strength and weak toughness so that its application is limited to certain extent. Various PPS alloys[2–6] were prepared to achieve mechanical improvements, whereas this kind of approach tends to give rise to more or less negative effect on thermal stability. Another reinforcement strategy is to fabricate composites by adding fillers such as fibers (glass fiber,[7] carbon fiber,[8,9] Kevlar fiber,[10] etc.) and nanoscale particles ($CaCO_3$,[11] SiO_2,[12] clay,[13] and Al_2O_3[14]). However, it is found that PPS/fiber composites often exhibit mechanical anisotropy for the orientation of fiber along the flowing direction in processing, and that PPS/particle composites are usually accompanied by residual stresses for the sharp-pointed edge of filled particles.

In recent years, carbon nanoscale tubes (CNTs) has played a successful candidate as reinforcement filler with high strength, low density, and great specific area,[15] which is often pretreated physically or chemically to reduce its strong tendency to conglomerate, usually modified by hydroxyl, carboxyl, or amino groups.[16] Multiwalled carbon nanotube (MWNT) is made of multilayer of coiling graphite, that is, 10–30 μm long and 10–50 nm in diameter,[17] which having been a focus in polymer composites research. As more and more kinds of polymer/CNT composites being studied,[16] the PPS/CNT system were also reported 2–3 years ago.[18–21]

Yang studied PPS/MWNT composites in which raw MWNTs leads to increased crystallization temperature (T_c) with MWNT content varying from 0.7 to 2 wt %, when the corresponding enthalpy (ΔH_c) getting decreased.[18] However, in studies on other polymer/CNT systems, there were reports that showed a decreased (rather than increased) T_c with increasing CNT content, when the corresponding ΔH_c almost keeping unchanged (in stead of decreasing). Díez-Pascual et al. characterized composites of poly(ether ether ketone) (PEEK) incorporated with single walled carbon nanotubes (SWNTs), on the surface of which certain amount of oxygenated groups were created through chemical treatment. In these PEEK/SWNT composites, T_c exhibited decreasing (while ΔH_c almost unchanged) with SWNT content increasing from 0.1 to 1 wt %, which was explained by CNT-confinement effect overweighing

CNT-inducing effect on crystal growth.[22] But such an explanation is not quite convincing, especially when CNT content is at such a low level. Considering that raw CNTs is usually more hydrophobic than pretreated CNTs, it seems that the affinity between CNT and polymer matrix plays a role that is not negligible in affecting T_c and ΔH_c of polymer/CNT composites.[23] Therefore, what will happen to PPS is interesting when MWNTs-OH is loaded instead of raw MWNTs.

For semicrystalline polymer composites, it is well known that T_c and ΔH_c have close relations with morphological structures such as crystallinity, crystallite size, and spherulite size, which contribute substantially to mechanical, thermal and chemical resistant properties. In general, higher crystallinity usually benefits thermal and chemical stabilities, and smaller crystallite size and spherulite size often result in better toughness. PPS/CNT composites are expected to achieve appreciable improvements to expend applications in such areas as automotive engine compartments and fuel pipeline systems, etc.[18] Therefore, it will not only be helpful in understanding but also in designing PPS/CNT composites to elucidate CNT nucleation effect in PPS.

The purpose of this study is to investigate MWNT-OH nucleation effect in PPS at low level of content. A series of PPS/MWNT-OH composites were prepared with MWNT-OH content ranging from 1 to 3 wt %. The MWNT-OH dispersion in PPS matrix was observed with the help of a scanning electronic microscope (SEM). By differential scanning calorimeter (DSC), the crystallization behavior was recorded to reveal MWNT-OH effect on enthalpy (ΔH_c) as well as crystallization temperature (T_c), which are thereby discussed in detail with a reasonable explanation proposed. The MWNT-OH effect on T_c was anticipated to be in agreement with the crystallite size measured by X-ray diffractometer (XRD), meanwhile the effect on ΔH_c was expected to be supported with the analyses of Fourier transformation infrared spectroscopy (FTIR) and X-ray photoelectron spectroscopy (XPS).

EXPERIMENTAL

Materials and Sample Preparation

Poly(*p*-phenylene sulfide) (PPS) injection powder, with T_m at 285°C, was purchased from Sichuan Deyang Chemical, China. The hydroxyl purified multiwall carbon nanotubes (MWNTs-OH), with 95% purity and more than 3.06 wt % hydroxyl group content, were made by Organic Chemical, Chengdu, China. The MWNT-OH length is about 10–30 μm, with outer diameter 20–30 nm and its special surface area is more than 200 m^2/g.

PPS was dried at 110°C for 2 h to remove water before blending with MWNTs-OH at 1, 2, and 3 wt %, respectively, by a mixer extruder Dynisco LME-230, at 300°C in 10 min, which was made twice for each sample.

Characterization

Scanning Electron Microscopy. SEM observation was conducted by means of a field-emission scanning electron microscope Hitachi S-4700 under the voltage of 20 kV. With each sample fractured in liquid nitrogen and covered with Pt, 10 SEM images were taken at different magnifications to assess the MWNTs-OH dispersion in PPS matrix.

Fourier Transformation Infrared Spectroscopy. FTIR spectrum was collected by a furrier transformation infrared spectrometer Nexsus 670 (Nicolet Analytical Instruments) under the resolution of 1 cm^{-1} in 128 scans.

X-Ray Photoelectron Spectroscopy. XPS spectra were measured with a X-ray photoelectron spectrometer VG ESCA Lab250, using the X-ray Al Kα (1486.6 eV) under the power of 300 W, and holding the sample chamber pressure less than 2×10^{-10} ψ. Setting the energy step size at 0.05 eV, the measured binding energy was calibrated based on the C1s binding energy 284.6 eV.

Differential Scanning Calorimetry. The crystallization behavior was described by a DSC Perkin–Elmer Pyris1. Each sample (about 5 mg) was first heated to 300°C at a heating rate 10°C/min, and then held at 300°C for 5 min to eliminate the thermal history. The nonisothermal crystallization behavior was recorded with the cooling curve from 300°C to 40°C at a cooling rate 10°C/min. Eventually, the second heating curves was proceeded at a heating rate 10°C/min from 40 to 300°C, exhibiting the trace of melting process.

Wide Angle X-Ray Diffraction. The WXRD patterns were scanned by an XRD D/max2500 VB2+/PC using Cu-Kα radiation source operated at 40 KV and 20 mA, with diffraction angle ranging from 3 to 40° at the speed of 5°/min.

RESULTS AND DISCUSSION

SEM Observation on MWNTs-OH Dispersion in PPS Matrix

The dispersion of carbon nanotubes in polymer matrix has a substantial influence on the properties of polymer/CNTs composites, which were herein examined with cryofractured samples by SEM.

Figure 1 shows typical SEM micrographs of PPS/MWNTs-OH system (3 wt % MWNTs-OH), which indicate clearly that the white spots MWNTs-OH are evenly and almost individually dispersed among the grey matrix PPS(with little MWNTs-OH bundled). No obvious agglomeration takes place in the PPS/MWNTs-OH composites when up to 3 wt % MWNTs-OH mixing with PPS under the blending condition mentioned earlier.

FTIR Evidence for Higher Degree of Crystallinity in PPS/MWCNT-OH Composites

Figure 2 exhibits the FTIR spectra of PPS and PPS/MWNTs-OH composites. It is found that each strong absorption band of the composites has almost no shift in comparison with that of PPS, except the band centered around 816.6 cm^{-1} and its shoulder band around 813.8 cm^{-1}, which are assigned to the out-of-plane bending vibration of S—Ar—S[24] and the bending vibration of benzyl ring, respectively. The former band moves from 816.6 to 817.7 cm^{-1}, 819.6 cm^{-1}, and 821.5 cm^{-1} with MWNT-OH content increasing from 0 to 1, 2, and 3 wt %, whereas the later band shifts from 813.8 cm^{-1} to 813.8 cm^{-1}, 811.9 cm^{-1}, and 810.0 cm^{-1}.

According to the IR interpretation principle for π–π bond, both the upwards shift of the band 816.6 cm^{-1} and the downwards shift of the band 813.8 cm^{-1} may probably be attributed to

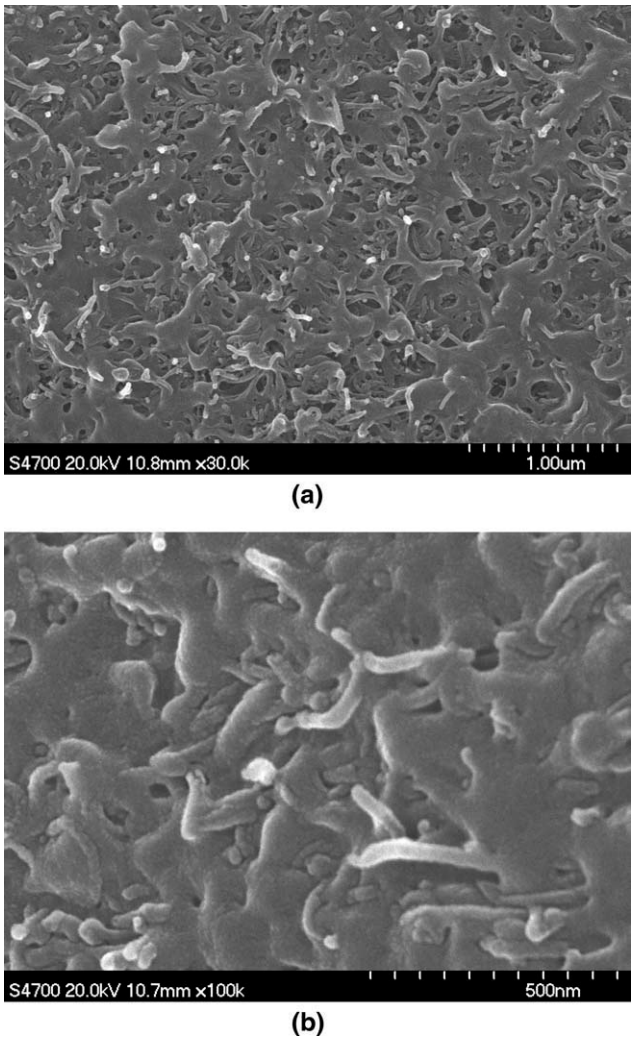

Figure 1. SEM micrographs for fractured surface of PPS/3% wt MWNTs-OH composites metallized with Pt overlayer at different magnifications.

stronger π-π bond interaction among S—Ar—S units, meaning more molecular units were packed tightly with each other and therefore indicating more PPS molecular chains were orderly rearranged into the crystal lattice, which is consistent with the result of DSC as shown in Table I.

XPS Evidence for Higher Degree of Crystallinity in PPS/MWNT-OH Composites

Figure 3 shows the XPS spectra of sulphur in PPS and PPS/MWNTs-OH composites, in which the peak centered around 163.5 eV is assigned to the binding energy of S2p.

Table I. Crystallite Size Indicator <*D*> for PPS and PPS/MWNTs-OH Composites

MWNT-OH content (wt %)	<*D*> /nm
0	12.6
1	11.5
2	10.5
3	9.5

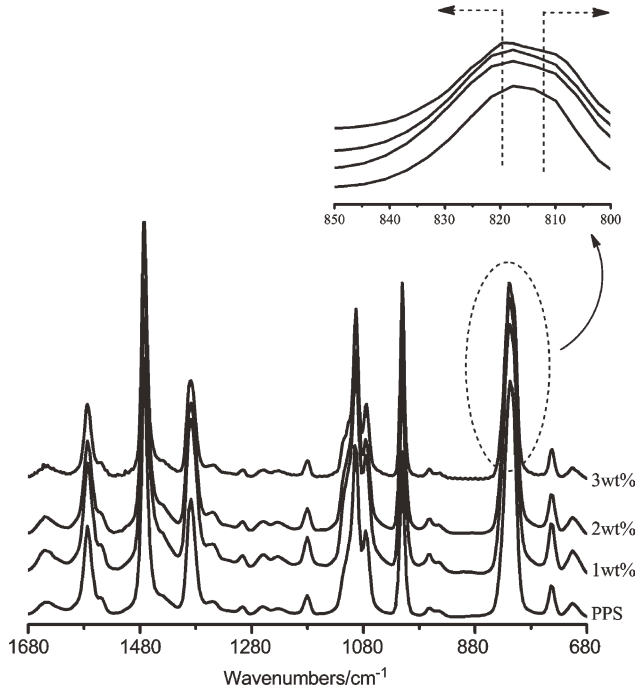

Figure 2. FTIR spectra of PPS and PPS/MWNTs-OH composites.

It is noticeable that there is a peak shoulder around 164.8 eV getting stronger with the content of MWNTs-OH increasing from 0 to 3 wt %. Such a peak-shoulder rising can be interpreted as the physico-chemical environment changing of sulfur[25] for more S—Ar—S units are rearranged into crystallites (as shown by data in Table I), in which more energy is needed for the S2p electron to overcome the surrounding energy barrier to escape.

WXRD Characterization

Figure 4 displays the WXRD patterns of PPS and PPS/MWNT-OH composites.

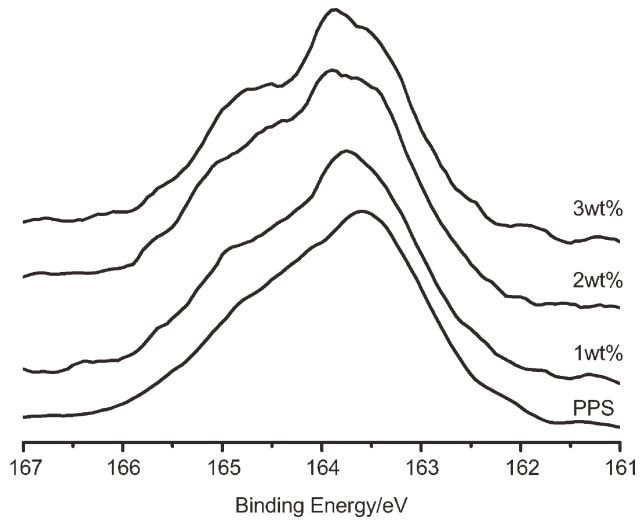

Figure 3. XPS spectra of PPS and PPS/MWNTs-OH composites.

Applied Polymer SCIENCE

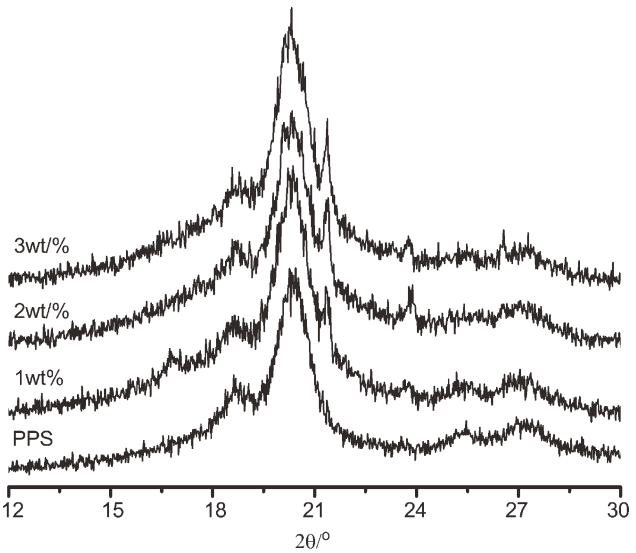

Figure 4. Wide-angle X-ray diffraction patterns of the PPS/MWNTs composites.

The crystallite size was estimated based on Derby-Scherrer expression [see eq. (1)].

$$D = \frac{k\lambda}{\beta \cos\theta} \tag{1}$$

where D is the crystallite size in the normal direction of the selected set of crystal planes, 2θ is the Bragg reflection angle of the corresponding set of crystal planes, k is the Derby-Scherrer constant ($k = 0.9$), λ is the X-ray wavelength ($\lambda = 0.1542$ nm for Cu-Kα radiation), and β is the calibrated half-width of Bragg reflection peak ($\beta = (B^2 - b_0^2)^{1/2}$, B is the experimental half-width of the peak, b_0 is the instrumental broadening factor, hereby $b_0 = 0.16^\circ$). Apparently, D is inversely proportional to β when θ is given, vice versa.

The diffraction peak at $2\theta \approx 20.4^\circ$ (see Figure 4) is assigned to the overlap Bragg reflections by the three sets of crystal planes of (200), (111), and (102).[26] Each set of crystal planes, according to Derby-Scherrer expression, corresponds to their own Derby-Scherrer expression, in which β_{200}, β_{111}, and β_{120} are inversely proportional to D_{200}, D_{111}, and D_{120}, respectively. Therefore, for the overlap peak, its half-width $\beta_{200\text{-}111\text{-}120}$ should basically have a negative correlation with crystallite size. If the left item D of Derby-Scherrer expression is defined as $<D>$ when the $\beta_{200\text{-}111\text{-}120}$ is taken as β in the right item, then $\beta_{200\text{-}111\text{-}120}$ also has a negative correlation with $<D>$ as shown by eq. (2). Thus $<D>$ should be a positive indicator (see Table I) for crystallite size.

$$< D >= \frac{k\lambda}{\beta_{200-111-120} \cos\theta} \tag{2}$$

It is found that the crystallite size indicator $<D>$ decreases with MWNTs-OH content increasing from 0 to 3 wt %, meaning crystallite size was progressively suppressed when MWNTs-OH increasingly dispersed in PPS matrix at low content.

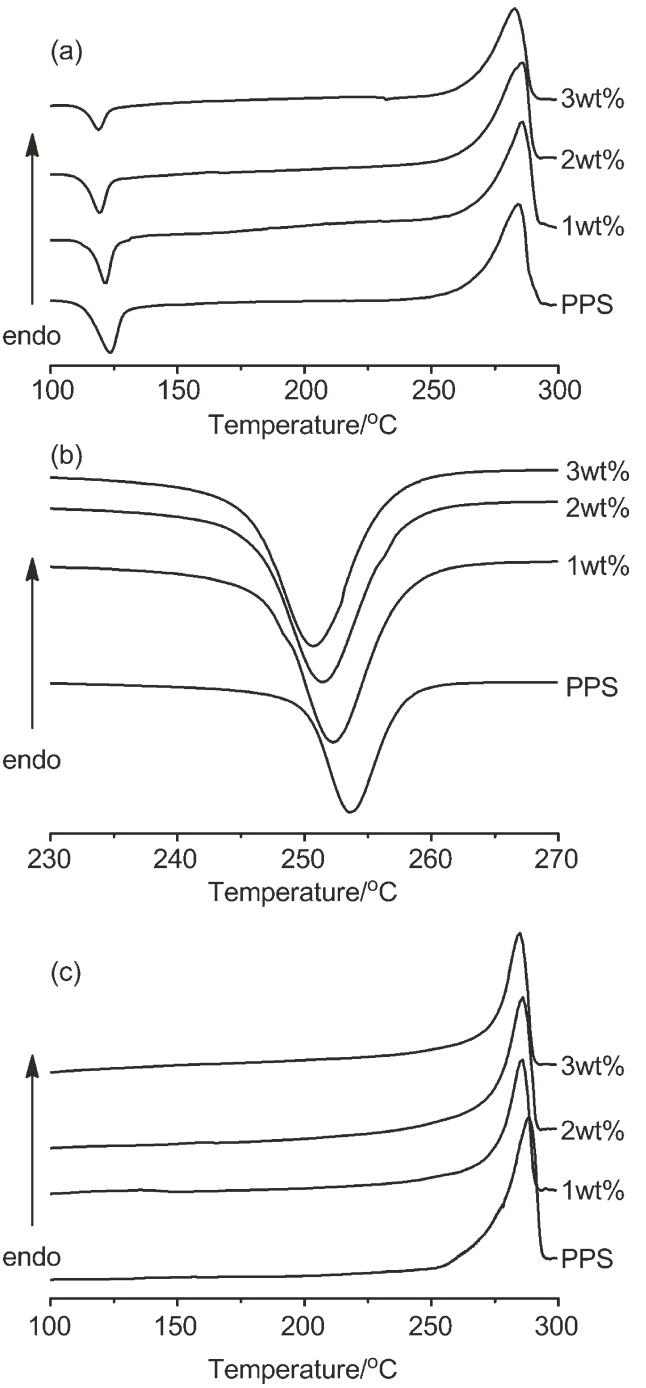

Figure 5. DSC curves of PPS and PPS/MWNTs-OH composites at cooling or heating rate of 10°C/min (a) first heating (b) cooling (c) second heating.

Crystallization and Melting Behaviors of PPS/MWNTs-OH Composites

The crystallization and melting behaviors of the studied composites were analyzed by DSC. Figure 5 presents the cooling and

Table II. Thermal Data of PPS and PPS/MWNTs-OH Composites

	Cooling		Second heating	
Samples	T_c/°C	ΔH_c/(J/g)	T_m/°C	ΔH_m/(J/g)
PPS	253.6	45.9	288.3	56.4
PPS-1 wt %MWNTs-OH	252.3	46.6	285.8	57.8
PPS-2 wt %MWNTs-OH	251.4	49.8	285.8	58.7
PPS-3 wt %MWNTs-OH	250.6	51.9	284.8	61.3

T_c, crystallization temperature; T_m, melting temperature; ΔH_c, crystallization enthalpy; ΔH_m, melting enthalpy.

second heating DSC traces, providing a series of thermal data listed in Table II.

Figure 5(a,b) show DSC cooling and second heating traces of pure PPS and PPS/MWNT-OH composites after eliminating thermal-history difference among samples, the thermal data of which are listed in the cooling and heating columns of Table II.

In cooling process, it is clear that the crystallization temperature (T_c) decreases from 253.6 to 252.3, 251.4, and 250.6°C for samples with MWNT-OH content varying from 0, to 1, 2, and 3 wt %, T_c shifting towards lower temperature with increasing MWNTs-OH content. Meanwhile, the crystallization enthalpy (ΔH_c) increases from 45.9 to 46.6, 49.8, and 51.9 J/g, indicating higher crystallinity obtained. Consequently, ΔH_c increases while T_c decreases with MWNTs-OH content increasing. The same tendency also applies to second heating process, where ΔH_m increases while T_m decreases with MWNTs-OH content increasing. Anyway, side-evidenced by FTIR and XPS analyses above, MWNTs-OH did serve as a nucleation agent in the light of higher crystallinity obtained even under progressively lowered T_c, suggesting heterogeneous nuclei sufficiently multiplied under the presence of well-dispersed MWNTs-OH.

However, the above results of PPS/MWNT-OH composites are contrary to what were found in PPS/MWNT composites as reported by Yang etc.,[18] in which raw MWNTs was used instead of MWNTs-OH. According to Yang, T_c of PPS/MWNT composites increases with the MWNT content increasing from 0 to 2 wt %, while both ΔH_c and ΔH_m decrease correspondingly. The hydroxyl groups on MWNTs-OH bring about two effects. On the one hand, because MWNTs-OH is less conglomerated than raw MWNTs, it tends to be better dispersed in PPS, leading to CNT network built up at even lower CNT content to hinder PPS chain fusing rearrangement. In contrast, poorer affinity of MWNTs-OH to PPS makes polymer chains more difficult to anchor steadily enough onto its surface to initiate crystal growing effectively, until lower temperature (T_c) is reached (meaning higher super-cooling temperature). Such result is in accordance with the XRD characterization for crystallite size (see "Crystallization and Melting Behaviors of PPS/MWNTs-OH Composites" section), from the point of view that the higher the supper-cooling temperature, the smaller the crystallite size. Therefore, there are probably two effects causing T_c decreasing with MWNT-OH increasing content: one is MWNT-OH network hindrance to PPS chain rearrangement, the other is MWNT-OH surface retardation to nuclear formation. Considering MWNTs has a good compatibility with PPS via "π-π stacking bond" that was evidenced with Raman spectra by Yang,[18,27] It seems that the MWNT-OH retardation effect is not negligible.

CONCLUSION

A series of PPS/ MWNTs-OH composites with MWNTs-OH well dispersed among PPS matrix were achieved through melt blending. At low MWNTs-OH content, higher crystallinity with smaller crystallite size was obtained when MWNTs-OH content increasing because of MWNTs-OH providing enough multiplied sites for crystal growing. Meanwhile, T_c decreases progressively, because it is not only the MWNTs-OH network, but also its poorer affinity to PPS that plays an important role in governing T_c of PPS/MWNTs-OH composites, which bearing a unique PPS/CNT morphology with potential applications.

ACKNOWLEDGMENT

This work was supported by the Fundamental Research Funds for the Central Universities China (ZZ1119).

REFERENCES

1. Hill, H. W.; Brady, D. G. *Polym. Eng. Sci.* **1976,** *16*, 831.
2. Lai, M. F.; Yang, Y. M. *J. Appl. Polym. Sci.* **2002,** *83*, 2906.
3. Sang, I. L.; Byoung, C. C. *Polymer* **1998,** *39*, 6441.
4. Yan, Y. G.; Li, Y. B. *Eur. Polym. J.* **2003,** *39*, 411.
5. Nam, J. D.; Kim, J. *J. Appl. Polym. Sci.* **2003,** *87*, 661.
6. Kubo, K.; Masamoto, J. *J. Appl. Polym. Sci.* **2002,** *86*, 3030.
7. Auer, C.; Kalinka, G.; Krause, T. *J. Appl. Polym. Sci.* **1994,** *51*, 407.
8. Kenny, J. M.; Maffezzoli, A. *Polym. Eng. Sci.* **1991,** *31*, 607.
9. Xu, H. Y.; Feng, Z. Z.; Chen, J. M. *Mater. Sci. Eng. A* **2006,** *416*, 66.
10. Yu, L. G.; Yang, S. R. *Thin Solid Films* **2002,** *413*, 98.
11. Wang, X. J.; Yang, J.; Long, S. R. Preprints of 3rd East Asian Polymer Conference; Sichuan University, Ed.; Chengdu, **2004**; p 254.
12. Lu, D.; Mai, Y. W.; Li, R. K. *Mater. Eng.* **2003,** *288*, 693.
13. Zou, H.; Xu, W.; Zhang, Q.; Fu, Q. *J. Appl. Polym. Sci.* **2005,** *99*, 724.
14. Schwartz, C. J.; Bahadur, S. *Wear* **2000,** *237*, 261.
15. Spitalsky, Z.; Tasis, D.; Papagelis, K.; Galiotis, C. **2010,** *35*, 357.

16. Morishita, T.; Matsushita, M.; Katagiri, Y.; Fukumori, K. *Prog. Polym. Sci.* **2010,** *48*, 2308.
17. Jeong, W.; Kessler, M. R. *Carbon* **2009,** *47*, 2406.
18. Yang, J. H.; Xu, T.; Lu, A. *Compos. Sci. Tech.* **2009,** *69*, 147.
19. Han, M. S.; Lee, Y. K.; Lee, H. S. *Chem. Eng. Sci.* **2009,** *64*, 4649.
20. Yang, J. H.; Xu, T.; Lu, A. *J. Appl. Polym. Sci.* **2008,** *109*, 720.
21. Yu, S. Z.; Wong, W. M.; Hu, X. *J. Appl. Polym. Sci.* **2009,** *113*, 3477.
22. Dıez-Pascual, A. M.; Naffakh, M.; Gomez, M. A. *Carbon* **2009,** *47*, 3079.
23. Li, L.; Li, C. Y.; Ni, C.; Rong, L. *Polymer* **2007,** *48*, 3452.
24. Zhou, X. Q.; Huang, Y. G.; Nie, F. *Mater. Rev.* **2008,** *22*, 364.
25. Rodriguez, J. A.; Li, S. Y.; Hrbek, J. *Surf. Sci.* **1997,** *370*, 85.
26. Napolitano, R.; Pirozzi, B.; Salvione, A. *Macromolecules* **1999,** *32*, 7682.
27. Zhang, Z. N.; Zhang, J.; Chen, P.; Zhang, B. Q. *Carbon* **2006,** *44*, 692.